Measurement of the differential $t\bar{t}$ production cross section in $p\bar{p}$ collisions at $\sqrt{s} = 1.96$ TeV with the D0 Detector

D0 Collaboration

(Dated: September 15, 2013)

The production of top quark-antiquark pair events in $p\bar{p}$ collisions at $\sqrt{s} = 1.96$ TeV is studied as a function of the transverse momentum and absolute rapidity of the top quarks as well as of the invariant mass of the $t\bar{t}$ pair. We select events containing an isolated lepton, a large imbalance in transverse momentum and four or more jets with at least one jet identified to originate from a b quark. Differential cross sections are corrected for detector effects assuming the standard model. The data sample corresponds to 9.7 fb^{-1} of integrated luminosity recorded with the D0 detector at RunII of the Fermilab Tevatron Collider. The single differential cross sections are in good agreement with SM predictions.

PACS numbers: 14.65.Ha, 12.38.Qk, 13.85.Qk

I. INTRODUCTION

The top quark [1, 2] is the heaviest of all elementary particles in the standard model (SM) with a mass of 173.2 ± 0.9 GeV [3]. The production of top quark-antiquark pairs ($t\bar{t}$) at the Fermilab Tevatron Collider (Tevatron) is dominated by the quark-antiquark ($q\bar{q}$) annihilation process. The measurement of $t\bar{t}$ differential production cross sections in $p\bar{p}$ collisions at the Tevatron provides a direct test of quantum chromodynamics (QCD), the theory of the strong interactions. Comparisons of differential cross sections with QCD deepen our understanding, and provide important information that can improve QCD simulations. A precise modeling of QCD is vital in many searches for contributions from new phenomena, where differential top quark cross sections are used to set constraints on new sources of physics. A precise understanding of the top quark production is also needed for measurements or searches involving rare processes in which other particles are produced in association with a $t\bar{t}$ pair or $t\bar{t}$ production is among the dominant backgrounds. A notable example of the latter case is a deviation of the observed charge asymmetry in $t\bar{t}$ production at D0 from SM predictions by more than 2.4 standard deviations [4]. This difference could be attributed to the exchange of a new heavy mediator, e.g., an axigluon [5, 6], that could also enhance the $t\bar{t}$ cross section. Differential cross sections, most notably as a function of the invariant mass of the $t\bar{t}$ pair $d\sigma/dm(t\bar{t})$, provide stringent constraints on axigluon models [7].

Previous measurements of differential $t\bar{t}$ production as a function of the transverse momentum of the t or $\bar{t}$ quark ($p_T^{\rm top}$) [8], and as a function of the invariant mass of the $t\bar{t}$ pair $m(t\bar{t})$ [7], have demonstrated good agreement with perturbative QCD (pQCD) calculations at next-to-leading (NLO), as well as next-to-next-leading order (NNLO) [9]. Compared to the previous D0 result, the current measurement employs a factor of ten more data allowing for more detailed tests of pQCD.

Differential cross sections are measured as a function of $m(t\bar{t})$, the absolute value of the rapidity $|y^{\rm top}|$, and $p_T^{\rm top}$,

using events with a topology corresponding to $t\bar{t}$ production. The "top" label in $|y^{\mathrm{top}}|$ and p_T^{top} refers to either t or $\bar{t}$ quarks. Events are selected in the lepton+jets decay channel, where the lepton (ℓ) refers to an electron or a muon. This channel corresponds to $t\bar{t} \to W^+\bar{b}W^-b$ decays, where one of the two W bosons decays leptonically ($W \to \ell\nu$), and the other hadronically ($W \to q\bar{q}'$). The events are therefore required to contain in addition to the lepton at least four jets and an imbalance in transverse momentum $\not{E}_T$[46], as discussed in section IV.

II.   MONTE CARLO SIMULATION AND QCD PREDICTIONS

Different Monte Carlo (MC) generators, implementing hard processes based on leading order (LO) and NLO QCD calculations, complemented with parton evolution and hadronization, are used to simulate detector effects by utilizing a detailed simulation of the D0 detector response based on GEANT [10]. The simulation is employed to determine the acceptance and the efficiency for selecting $t\bar{t}$ events, to extract a migration matrix, needed to unfold detector effects, and to estimate systematic uncertainties associated with the measurements. The $t\bar{t}$ signal samples are generated with MC@NLO+HERWIG [11, 12] and ALPGEN+PYTHIA [13, 14]. The CTEQ6M parton distribution functions (PDF) [15] are used for MC@NLO, with a factorization and renormalization scale of $\mu = \sqrt{\sum(m^2 + p_T^2)}$, while parton showering is performed with HERWIG. All final-state partons are summed up for the chosen scale, except the decay products of the W boson. The ALPGEN samples are generated using the CTEQ6L1 PDF [16], with the same scale but employing PYTHIA for the parton shower.

Several QCD predictions for differential $t\bar{t}$ cross sections have been calculated at higher orders than those included in the MC generators: two different approximate NNLO calculations based on next-to-next-leading logarithm (NNLL) resummation for $m_t = 173$ GeV [9, 20], and using $m_t = 172.5$ GeV [21], both use the MSTW2008NNLO PDF [22]. The renormalization and factorization scale μ (also referred to as "scale") used to calculate $m(t\bar{t})$ is higher than m_t. Employing m_t as scale leads to large and negative NLO corrections, that results in a negative differential cross section at NLO especially at large $m(t\bar{t})$. Instead, the authors choose the higher scale $m(t\bar{t})$. This scale choice avoids the previously described issue, but leads to a lower overall inclusive cross section.
The following processes contribute to the background, and are estimated from MC.

A.   *W*+jets events

Samples of W+jets events with a W boson are generated with ALPGEN [13] using the CTEQ6L1 PDF. The scale is set to $\sqrt{m_W^2 + \sum(m^2 + p_T^2)}$ and the parton shower is simulated with PYTHIA. The p_T of the W boson in MC is calibrated to $\ell+ \not{E}_T$ control data. The W+jets sample consists of events where one W boson is produced via an electroweak interaction, together with additional partons from QCD processes. The W+jets final state can be split into four subsamples according to parton flavor: $Wb\bar{b}$ + jets, $Wc\bar{c}$ + jets, Wc + jets and W+ light jets, where light refers to u, d, s quarks or gluons. The LO ALPGEN predictions are corrected for NLO effects as provided by MCFM [17]: the W + jets cross section is multiplied by a "k-factor" of 1.30, and the $Wb\bar{b}$ + jets and $Wc\bar{c}$ + jets cross sections have an additional heavy-flavor k-factor of 1.47 [18].

B.   *Z*+jets events

Z+jets events with a Z boson decaying to an electron, muon or tau pair, are also generated with ALPGEN, using the same PDF, scale and parton showering as for the W+jets samples (but with the p_T of the Z boson calibrated to dilepton control data). The LO ALPGEN predictions are corrected for NLO effects as provided by MCFM [17]: the Z+jets cross section is multiplied by a k-factor of 1.30, and the $Zc\bar{c}$ + jets and $Zb\bar{b}$ + jets cross sections by an additional heavy-flavor k-factor of 1.67 and 1.52, respectively [18].

C.   Single top events

Single top-quark production through the s and t-channels are generated with the COMPHEP MC generator [19] and use the CTEQ6L1 (s-channel) and CTEQ6M (t-channel) PDF. The scale is set to m_t (s-channel) and $m_t/2$ (t-channel).

The s and t-channel contributions are normalized to the NLO cross sections of 1.04 and 2.26 pb [19], respectively. The uncertainty on the cross section is set to 12.6% (taken from changes in scale by factors of 2 and $\frac{1}{2}$. The top quark mass in the single top quark samples is set to 172.5 GeV. As the single top quark background represents only a small contribution to the sample composition, no effects are considered from the dependence of this background on m_t.

D. Diboson events

Diboson production (WW, WZ and ZZ bosons) is generated with PYTHIA [14], using CTEQ6L1 PDFs, with a scale of $\sqrt{m_V^2 + \sum(m^2 + p_T^2)}$, V refers to the leptonically decaying W or Z boson. These processes are normalized to NLO cross sections, calculated with MCFM [17], of 11.62 pb, 3.25 pb and 1.33 pb, respectively. An uncertainty of 7% on the cross section is assigned, corresponding to half the difference between the LO and NLO predictions.

III.   THE D0 DETECTOR

The D0 detector [23] consists of several subdetectors designed for identification and reconstruction of the products of $p\bar{p}$ collisions. A silicon microstrip tracker (SMT) and central fiber tracker surround the interaction region for pseudorapidities $|\eta| < 3$ and $|\eta| < 2.5$, respectively. These elements of the central tracking system are located within a 2 T superconducting solenoidal magnet, providing measurements for reconstructing event vertices and trajectories of charged particles. The SMT [24, 25] strip pitch of 50-80 μm provides reconstruction of the primary interaction vertex (PV) with a precision of about 40 μm in the plane transverse to the beam direction, dominated by the beam size of 30 μm. The impact parameter of any trajectory relative to the PV is determined with a precision between 20 and 50 μm depending on the number of SMT hits and p_T, which corresponds to the key component of lifetime-based identification of jets containing b quarks. Particle energies are measured using a liquid argon and uranium calorimeter that is segmented into a central calorimeter covering $|\eta| < 1.1$, and two end calorimeters extending the coverage to $|\eta| < 4.2$. Outside of the calorimetry, trajectories of muons are measured using three layers of tracking detectors and scintillation trigger counters, and 1.8 T iron toroidal magnets between the first two layers. In front of the end-calorimeter cryostats, plastic scintillator arrays provide measurements of luminosity.

IV.   EVENT SELECTION AND SAMPLE COMPOSITION

This analysis uses all the data recorded with the D0 detector in RunII corresponding to 9.7 fb^{-1} of integrated luminosity, with all requirements on data quality satisfied.

The trigger selects ℓ+jets events by requiring at least one lepton (electron or muon) or a lepton and a jet with an efficiency of 95% or 80% for $t\bar{t}$ events containing an electron or muon candidate, respectively. Accepted events require the presence of a PV within 60 cm of the center of the detector along the beam axis, one isolated electron (or muon) with $p_T > 20$ GeV and $|\eta| < 1.1$ (or $|\eta| < 2$), $\not{E}_T > 20$ GeV, and at least four jets with $p_T > 20$ GeV and $|\eta| < 2.5$. The leading jet is required to have $p_T > 40$ GeV. To suppress jets from additional collisions in the same bunch crossing, jets are required to contain two tracks consistent with emanating from the PV (vertex confirmed jets). A minimum separation in azimuth is imposed between the momentum of the lepton and $\not{E}_T$, to reduce multijet background caused by the missidentification of a jet as a lepton and the consequent impact on the accompanying $\not{E}_T$. At least one of the jets is selected as likely to originate from a b quark (b tagged) using a multivariate discriminant (MVD) [26, 27]. The discriminant combines variables that characterize the presence and properties of secondary vertices and tracks within jets. The MVD identification of jets containing b quarks has an efficiency of approximately 60%, with a misidentification rate of $\approx 1.2\%$. The $t\bar{t}$ events selected in the ℓ+jets decay channel also contain contributions from electrons and muons stemming from the decay of τ leptons ($t \to Wb \to \tau\nu_\tau b \to \ell + \nu_\ell \nu_\tau b$). Events containing two or more leptons are rejected.

The background contributions originate from processes with different final states that are misidentified (instrumental background) and irreducible background from processes with final states similar to $t\bar{t}$. Data-driven [28] and MC methods are employed to model the instrumental background. A description of the data-driven methods can be found in Ref. [29]. Instrumental background arises either from $t\bar{t}$ events where both W bosons decay leptonically, but only one of the leptons is identified, or from multijet processes where a jet is misidentified as an electron in the e+jets channel, or a muon originating from the decay of a heavy quark appears to be isolated in the μ+jets channel. The

irreducible background processes are estimated using MC, as described in detail in Sec. II. Most of this background arises from W+jets production, and to constrain it, we use the exclusive two and three-jet ℓ+jets data, dominated by W+jets production, in addition to the inclusive four-jet multiplicity bin (dominated by $t\bar{t}$). We determine the sample composition from a simultaneous fit for the $t\bar{t}$ cross section and for the heavy-flavor contribution from W+jets to the data. The fit employs the MVD b identification output distribution for the two, three, and inclusive four-jet multiplicity bins. It yields a W+jets heavy-flavor scale factor $s_{\text{fit}}^{\text{WHF}} = 0.89 \pm 0.08$ to be applied to the $Wb\bar{b}$ + jets and $Wc\bar{c}$ + jets contributions in addition to the NLO k-factors discussed in Sec. II. Similar procedures were used in previous measurements by D0, for example [29]. The simultaneous fit to the exclusive two, three, and inclusive four-jet multiplicity bins yields a $t\bar{t}$ cross section of $\sigma_{\text{fit}}^{t\bar{t}} = 8.00 \pm 0.40$ pb. There is no need for an additional scale factor to accommodate the Z+jets heavy-flavor contributions. These parameters are applied to the MC, which is used to measure the $t\bar{t}$ differential cross section using inclusive four-jet data.

The total inclusive $t\bar{t}$ cross section is also calculated from the differential measurement by summing up all bins of the cross section (see Secs. IX and VII). This yields a value of $\sigma_{\text{tot}}(p\bar{p} \to t\bar{t}) = 8.27 \pm 0.48(\text{stat.}) \pm_{0.77}^{0.79} (\text{syst.})$ pb, measured using only events with at least four jets. This value is compatible with the cross section measured by the simultaneous fit using also events with two or three jets, but slightly larger. In the figures presented below, the $t\bar{t}$ predictions are normalized using the cross section measured using events with at least four jets. Figures 1 and 2 demonstrate, respectively, the quality of the modeling of the selected events in the e+jets and μ+jets events with the background and signal contributions for (a) the number of jets, (b) the scalar sum H_T of the p_T of the lepton and jets, (c) $\not\!\!E_T$ and (d) lepton p_T distribution. The composition of the selected data is given in Table I.
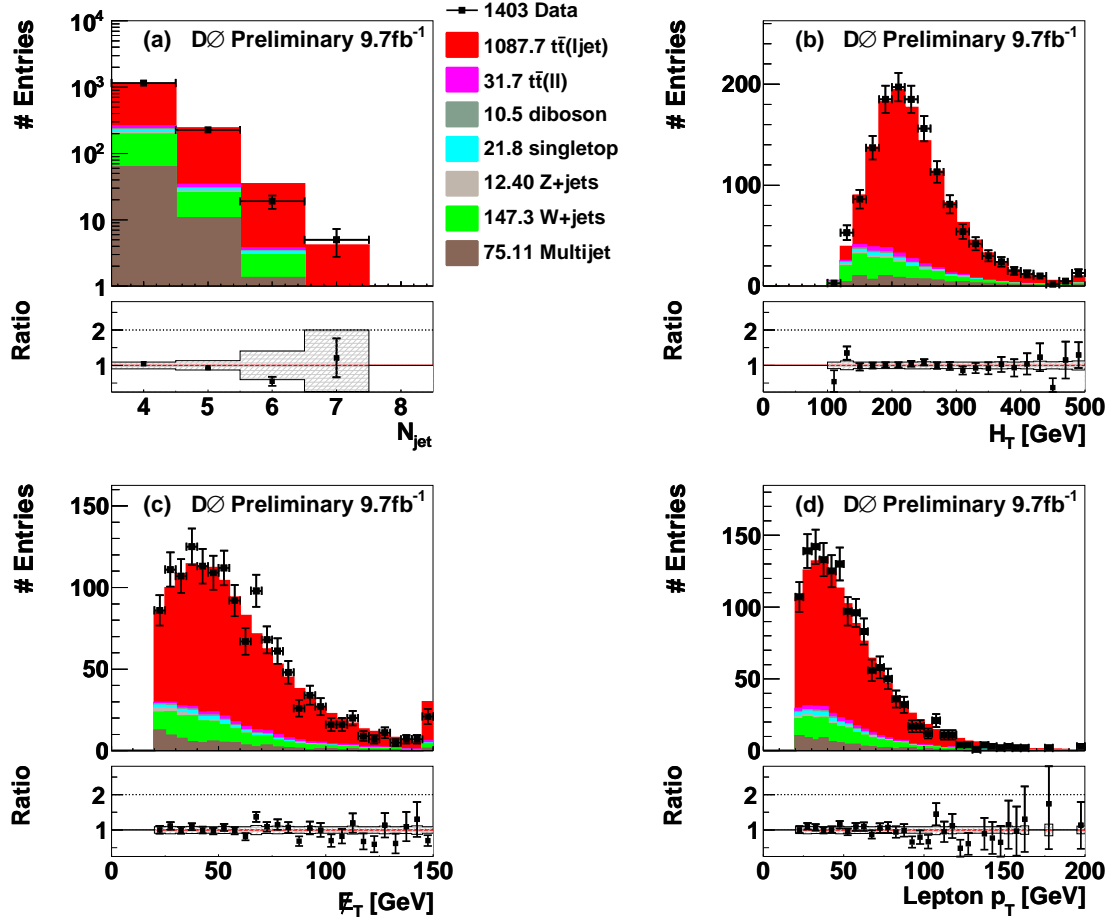

FIG. 1: Number of selected events for the e+jets final state as a function of (a) the number of jets, (b) H_T, (c) $\not\!\!E_T$ and (d) lepton p_T, assuming the measured inclusive $t\bar{t}$ cross section of 8.27 pb. The ratios of data to the sum of all background contributions are shown in the panels below the distributions. The shaded bands show the 1 s.d. systematic uncertainties for the combined signal and background contributions.
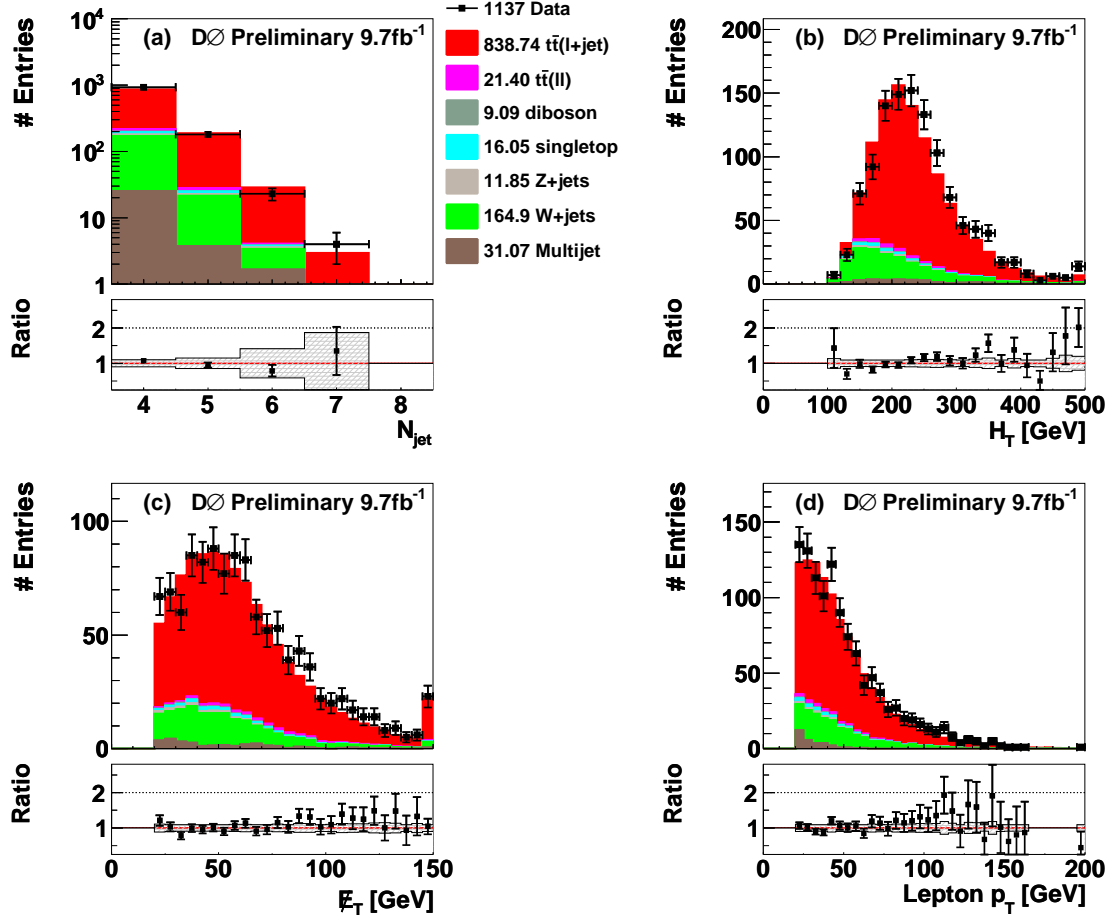
FIG. 2: Number of selected events for the μ+jets final state as a function of (a) the number of jets, (b) H_T, (c) $\not{E}_T$ and (d) lepton p_T, assuming the measured inclusive $t\bar{t}$ cross section of 8.27 pb. The ratios of data to the sum of all background contributions are shown in the panels below the distributions. The shaded bands show the 1 s.d. systematic uncertainties for the combined signal and background contributions.

V.   MEASUREMENT TECHNIQUE

Measuring any cross section involving t quarks benefits from the very short lifetime of the t quark, in that it decays before it can hadronize. Effects of hadronization and QCD corrections are therefore reduced. Moreover, at Tevatron energies, the transverse momentum of $t\bar{t}$ pairs is almost always smaller than $m(t\bar{t})$ and production is central, so that almost the entire phase space is within the acceptance. Corrections as well as their uncertainties are small leading to well measured top-quark cross sections.

The differential cross-sections are defined in terms of t quarks and corrected for detector and QCD effects using a regularized matrix unfolding procedure [30, 31]. This procedure reduces the influence of model dependencies in the cross section determination. It introduces correlations among the bins used in the measurement, which are reduced by regularization. Unfolding event migrations relies on a migration matrix (A), which describes the relation between the true distribution of a variable ($\vec{x}_{\text{true}}$) and its reconstructed distribution ($\vec{y}_{\text{rec}}$) as $A \cdot \vec{x}_{\text{true}} = \vec{y}_{\text{rec}}$. Each matrix element A_{ij} is the probability for an event originating from bin j of $\vec{x}_{\text{true}}$ to be measured in bin i of $\vec{y}_{\text{rec}}$. The migration matrix is based on the simulated performance of the D0 detector. It has twice as many bins as used at the reconstruction level at the generator level, to provide detailed information on the bin-to-bin migrations, which can improve the accuracy of the unfolding [32]. The true distribution $\vec{x}_{\text{true}}$ can be estimated using $A^{\dagger}$, the pseudoinverse [33] of the matrix A: $\vec{x}_{\text{true}} = A^{\dagger} \cdot \vec{y}_{\text{rec}}$. As with plain matrix inversion, this results in large contributions that lack statistical significance. Such contributions can be minimized by imposing regularization, which leads to an effective cutoff of the insignificant terms. We regularize the unfolding as implemented in *TUnfold* [34]. The regularization

TABLE I: Number of expected events contributing from each source in the e+jets and μ+jets decay channels for events with at least four jets (uncertainties are statistical).

Process	μ+jets	e+jets
Multijet	31.1 ± 10.0	75.1 ± 13.0
W+jets	164.9 ± 3.1	148.8 ± 2.6
Diboson	9.1 ± 0.3	10.5 ± 0.3
Z+jets	11.85 ± 0.4	12.4 ± 0.4
Singletop	16.05 ± 0.2	21.8 ± 0.3
$t\bar{t}$ ($\ell\ell$)	22.6 ± 0.2	33.5 ± 0.3
$\sum$ backgrounds	254.4 ± 10.5	302.1 ± 13.3
$t\bar{t}$ (ℓ+jets)	838.7 ± 3.2	1088.7 ± 3.8
Data	1137	1403

is based on the derivative of the distribution and is done in twice as many bins as shown in the final results. The value of the regularization strength is determined using the so-called L-curve approach that balances the consistency of x with the data against the scatter of x. An insufficient regularization causes fluctuations in the unfolded result, where as excessive regularization overly biases the measurement towards the MC generated distribution. A systematic uncertainty is derived for this procedure within these bounds (see Sect. VII).

VI. EXTRACTION OF SIGNAL

For the reconstruction of the four-vectors of the full $t\bar{t}$ decay chain $t\bar{t} \rightarrow Wb + W\bar{b} \rightarrow (q'\bar{q})b + (\ell\nu)\bar{b}$; we use a constrained kinematic reconstruction algorithm [35] that takes into account experimental resolution. The masses of the W boson and the t quark are fixed to 80.4 GeV and 172.5 GeV, respectively. $\not{E}_T$ provides only an initial estimate for the p_T of the neutrino. The longitudinal momentum $p_z(\nu)$ is estimated by constraining the W boson mass from its decay products to 80.4 GeV. This yields a quadratic equation in $p_z(\nu)$ with two solutions. These solutions, together with the 12 possible jet–quark assignments yield 24 possible solutions. This number of solutions is reduced by preferably assigning b tagged jets to b quarks. The solution with the best χ^2 for assigning the reconstructed objects to the parton level quantities is used for the input to the unfolding (see Sec. V). To check the modeling, the distributions in χ^2 for data are compared in Fig. 3 to expectations for the (a) e+jets and (b) μ+jets final state.

In the following the modeling of signal and background processes is verified through a comparison of the data to the
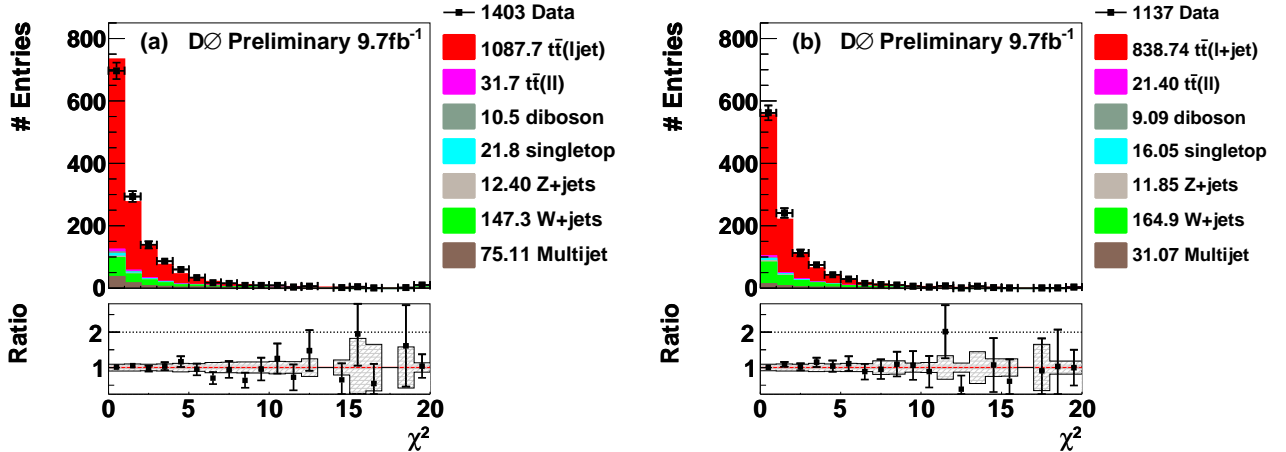

FIG. 3: Number of fitted events as a function of χ^2 from the kinematic reconstruction for the (a) e+jets and (b) μ+jets final states, assuming the measured inclusive $t\bar{t}$ cross section of 8.27 pb. The shaded bands show the 1 s.d. systematic uncertainties for the combined signal and background contributions.

number of expected $t\bar{t}$ signal events by MC@NLO+HERWIG and the sum of all background contributions. Figures 4 to
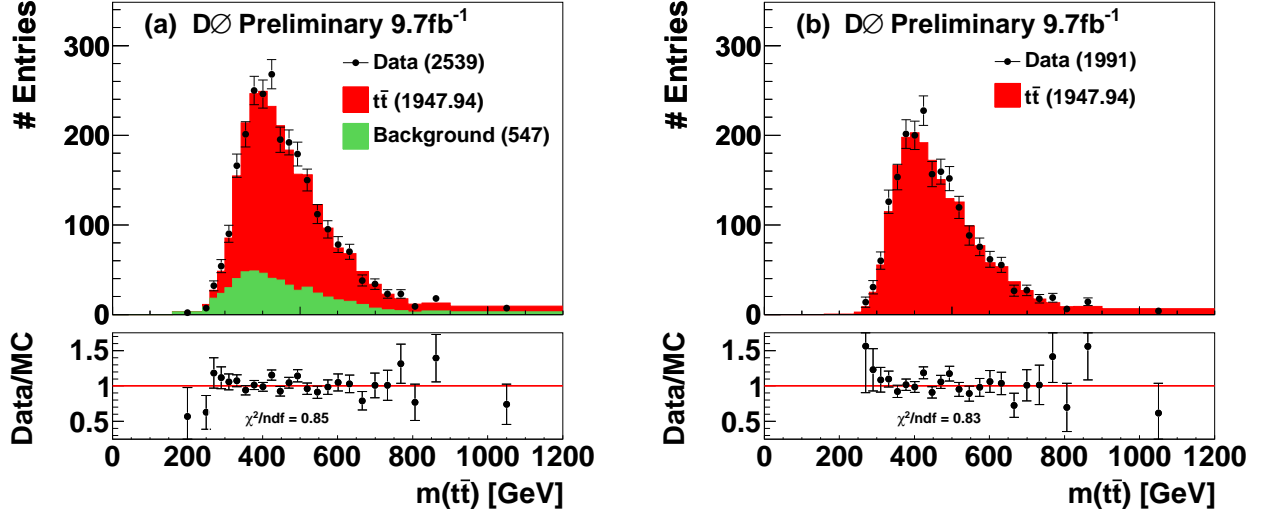
FIG. 4: Number of selected data events as a function of $m(t\bar{t})$, (a) compared to the sum of contributions from signal and background processes, and (b) the background-subtracted distribution.

6 show the distributions before unfolding, i.e., the input $m(t\bar{t})$ (Fig. 4), $|y^{\text{top}}|$ (Fig. 5), and p_T^{top} (Fig. 6). The $|y^{\text{top}}|$ and p_T^{top} distributions contain both $W \to \ell\nu$ and $W \to \bar{q}q'$ decay modes. Similar resolutions suggest a combination of these distributions during unfolding. The distribution in (a) of Fig. 4 to 6 shows the data compared to the $t\bar{t}$ signal and background processes, and (b) shows the background-subtracted data. The lower panels indicate the ratio of the data to the sum of all contributions. The $t\bar{t}$ contribution is normalized to the measured inclusive cross section of 8.27 pb (see Eq. (1) in Sec. VII). The data and its description by the sum of signal and background processes agrees within uncertainties.
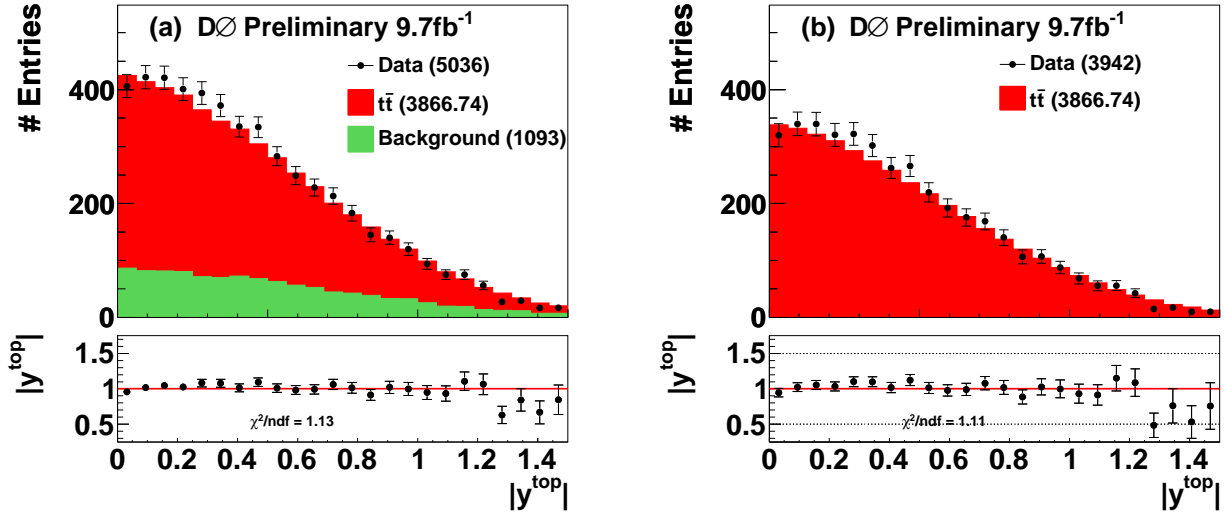

FIG. 5: Number of predicted and observed data events as a function of $|y^{\text{top}}|$, more details in caption of Fig. 4.
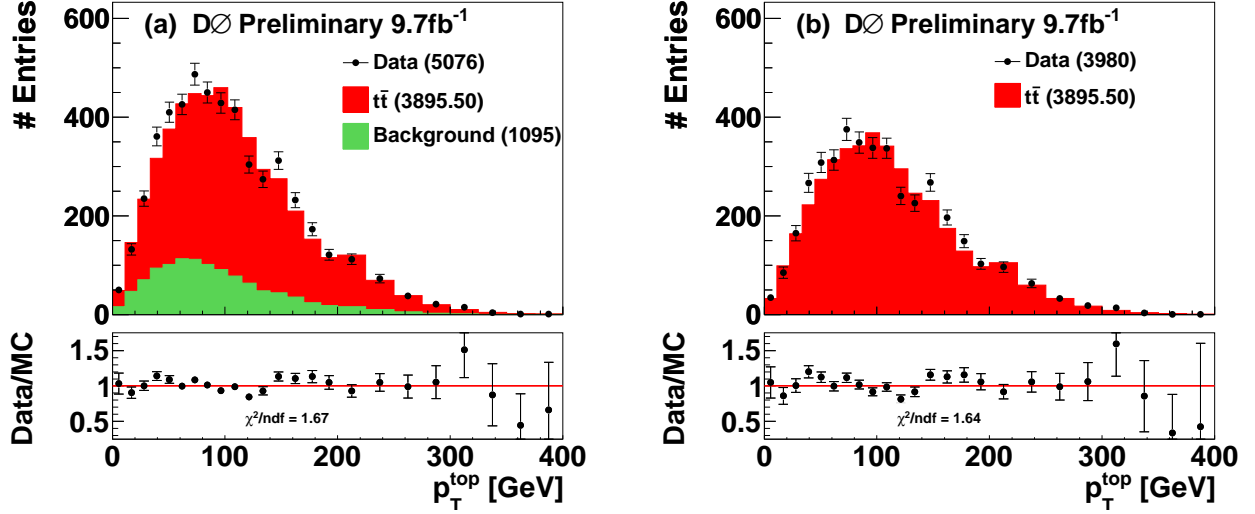
FIG. 6: Number of predicted and observed data events as a function of p_T^{top}, more details in caption of Figure 4.

VII.   CROSS SECTION DETERMINATION

Equation 1 is used to calculate the differential $t\bar{t}$ cross section as a function of the quantity X_i, where i denotes an individual bin, and ΔX_i its width.

$$\frac{d\sigma}{dX_i} = \frac{N_i^{\mathrm{signal}}}{\epsilon_i \cdot \mathcal{L} \cdot \mathcal{B} \cdot \Delta X_i} \; . \tag{1}$$

The unfolded N^{signal} is corrected for detector efficiency ϵ (that includes the kinematic acceptance $\mathcal{A}$), for the total integrated luminosity $\mathcal{L}$ that corresponds to the selection requirements, including data quality, and for the branching fraction $\mathcal{B}$ into the ℓ+jets decay channels [36]. The branching fractions include electrons and muons originating from the decay of τ leptons. Results are shown in Fig. 7 to 9, respectively, for $m(t\bar{t})$, $|y^{\mathrm{top}}|$, and p_T^{top}, and t and $\bar{t}$ are summed in the combined cross section. The differential cross section in each bin of these variables is given in Tab. III to V in App. A. No bin centering correction is applied to the measurements, and the cross sections are displayed at the center of each bin. The number of expected background events, as estimated through MC or data-driven methods, are subtracted from the data. The number of background-subtracted events (N^{signal}) is corrected for effects from limited detector resolution by means of the regularized matrix unfolding as discussed in Sec. V.

VIII.   SYSTEMATIC UNCERTAINTIES

The systematic uncertainties are assessed by changing the values of any specific parameter in the modeling of the data, and repeating the analysis. Unless stated to the contrary, these modifications and their impact employ the uncertainties obtained from alternative calibrations of the MC. The migration matrix and the background contributions are extracted from these different models, while the regularization strength is fixed relative to the nominal unfolded data. The difference between the nominal unfolded data and unfolded data, including a systematic modification, defines a source of systematic uncertainty. Individual sources of systematic uncertainty are added in quadrature for each bin of a differential cross section. Usually, the largest uncertainties arise at large values of $m(t\bar{t})$, $|y^{\mathrm{top}}|$, or p_T^{top}, where there are few events.

A. Modeling of signal

The effect of NLO corrections to the matrix element for $t\bar{t}$ production is estimated by comparing $t\bar{t}$ events simulated with MC@NLO, with parton showering through HERWIG, to ALPGEN, with parton showering through PYTHIA. In this comparison, the contribution arising from the use of an alternative model of hadronization is expected to have a smaller impact, as was checked by studying the difference between ALPGEN+PYTHIA and ALPGEN+HERWIG. An additional uncertainty on signal arises from poor modeling of the reconstructed $p_T^{t\bar{t}}$ at D0 [4], in contrast to results from CDF, ATLAS and CMS, where good agreement is observed [37–39]. A systematic uncertainty is estimated by reweighting the distribution of reconstructed the $p_T^{t\bar{t}}$ in MC to the one observed in data. Additionally, the value of m_t is changed within its uncertainty of $\delta(m_t) = \pm 1$ GeV, reflecting the latest combined measurements by D0 and CDF [3].

B. Parton distributions functions

The uncertainty on the PDF used to describe the initial parton distributions is estimated by reweighting the MC according to each of the 20 error eigenvectors of the CTEQ6M PDF according to the procedure described in [15], with their effects added in quadrature.

C. Modeling of detector

Uncertainties from modeling the detector include uncertainties on trigger efficiency, lepton identification and b-quark identification. The uncertainty on trigger efficiency is roughly 2.5% for harder collisions ($p_T^{\text{top}} > 90$ GeV or $m(t\bar{t}) > 505$ GeV) and 6% for softer collisions that are typically closer to trigger thresholds. The p_T^{top} and $m(t\bar{t})$ differential cross-sections are modified according to these uncertainties, and the $|y^{\text{top}}|$ differential cross section is rederived with trigger efficiencies modified according to p_T^{top}. The identification efficiencies for b, c, uds quarks, and gluons in MC are calibrated with reference to the results in dijet data. Additional uncertainties arise from track multiplicity requirements on the selected jets in the identification of b quarks.

Other uncertainties from modeling the detector arise from the calibration of the jet energy, resolution and efficiency. The jet energy scale (JES) [40] corrects the measured energy of the jet to the energy of its constituent particles prior to interaction with the detector. The JES is derived using a quark jet dominated γ + jet sample, and corrects for the difference in detector response between data and MC. An additional correction based on single particle response accounts for the different characteristics of quark and gluon jets. Jets in MC have their energies smeared so that the simulated resolution matches the one observed in data. The jet reconstruction and identification efficiency in MC is calibrated to that observed in dijet data. The jet vertex confirmation efficiency (see Section IV) in MC is calibrated to the one in dijet data.

D. Sample composition

Uncertainties on the composition of the selected events arise from the heavy-flavor scale factor in W+jets, the estimates of misidentified leptons, and the uncertainty on the $t\bar{t}$ cross section. A systematic uncertainty of 8% is applied on the normalization of the $Wc\bar{c}$ + jets and $Wb\bar{b}$ + jets processes, obtained from a simultaneous fit to the MVD distribution in the two, three, and inclusive four-jet multiplicity bins (Sec. IV). The uncertainties on the data-driven method of estimating multijet (MJ) background and its kinematic dependencies, mostly due to the uncertainties on the selection rates of true and false lepton candidates, are 0.172 in μ+jets final states and 0.046 in e+jets final states [41]. As described in Sec. IV, the $t\bar{t}$ cross section is fitted simultaneously for the heavy-flavor scale factor and has a relative uncertainty of 5% corresponding to the $t\bar{t}$ cross section of 8.00 ± 0.40 pb, in agreement with the result from the inclusive $t\bar{t}$ differential cross section of this paper. A systematic uncertainty is included by changing the level of the background-subtracted data by $\pm 5\%$. An overall 6.1% uncertainty on $\mathcal{L}$ [42] is assigned to the unfolded cross section data. This effects yields from signal and background in the same way.

TABLE II: Sources of systematic uncertainties. The uncertainty due to each source on the inclusive cross section is given in columns two and three in %. The effects on the bins of the differential cross section are in the range given in the last column.

Source of uncertainty	Relative uncertainties [%]		
	$\delta_{\text{incl,rel}}^{\text{up}}$	$\delta_{\text{incl,rel}}^{\text{down}}$	rel. unc.
Alternative model for signal	+5.17	−4.28	$3 - 13$
PDF (CTEQ6M 20 error sets)	−2.96	+3.38	$1 - 4$
Lepton identification	+0.51	−0.53	$1 - 3$
Jet energy scale	+2.41	−2.50	$1 - 20$
Jet energy resolution	+0.37	−0.38	$1 - 2$
Jet identification	+0.31	−0.31	$1 - 2$
Jet flavor correction	−0.91	+0.76	$1 - 6$
b identification	+1.38	−1.40	$1 - 3$
Vertex confirmation	−0.36	+0.36	$1 - 1$
Dependence on m_t	+0.32	−0.35	$1 - 2$
Mismodeling of $p_T^{t\bar{t}}$	+0.79	−0.67	$1 - 4$
Trigger efficiency	+2.64	−2.64	$2.5 - 6$
Luminosity	+6.10	−6.10	$6 - 6$
W+jets heavy-flavor scale factor	+0.75	−0.78	$2 - 8$
True and false lepton efficiencies	+0.55	−0.57	$1 - 2$
Assumed $t\bar{t}$ cross section	+1.58	−1.47	$1 - 3$
Procedural (unfolding)	+0.18	−0.18	$1 - 2$
Total systematic uncertainty	+9.62	−9.29	−

E. Regularization strength

As a procedural uncertainty of the unfolding method, the regularization strength (Sec. V) is changed within its uncertainty, and its impact added to the uncertainty of the procedure.

IX. CROSS SECTIONS

The inclusive $t\bar{t}$ production cross section in the ℓ+jets decay channel is measured from the differential cross section in inclusive four-jet events to be:

$$\sigma_{\text{tot}}(p\bar{p} \to t\bar{t}) = 8.27 \pm 0.48(\text{stat.}) \pm_{0.77}^{0.79}(\text{syst.}) \text{ pb.} \tag{2}$$

This result is in agreement with the inclusive result of Sec. IV, which was based on the exclusive two, three, and inclusive four-jet multiplicity bins. The result of Eq. (2) is compared to the fully resummed NNLL at NNLO QCD calculation (using $m_t = 172.5$ GeV and the MSTW2008NNLO PDF), which finds $\sigma_{\text{tot}}^{\text{res}} = 7.24_{-0.27}^{+0.23}(\text{scales} + \text{pdf})$ pb [43]. The differential predictions [21] and MC@NLO are renormalized to match the inclusive cross section of this calculation. The total cross section of the approximate NNLO calculation [9, 20] gives $7.08_{-0.24}^{+0.20}(\text{scales})_{-0.27}^{+0.36}(\text{PDF})$ pb for a t quark mass of 173 GeV as calculated from the prediction for p_T^{top}, without a change in absolute normalization. The first uncertainty is given by the independent change in μ and the latter by the uncertainties from the choice of PDF. It should be noted that, using the same framework, but using the CT10 [44] PDF, yields a somewhat larger $t\bar{t}$ cross section: $7.38_{-0.25}^{+0.14}(\text{scales})_{-0.32}^{+0.45}(\text{PDF})$ pb [9]. The data are also compared to differential cross section predictions from MC@NLO and ALPGEN yielding a total cross section of $\sigma_{\text{tot}} = 7.54$ pb and $\sigma_{\text{tot}} = 5.61$, respectively.

Contributions beyond the highest bin boundary are included in the last bin of the $m(t\bar{t})$, $|y^{\text{top}}|$ and p_T^{top} distribution. Figure 7 (a) shows the cross section for the unfolded data (black circular markers) as a function of $m(t\bar{t})$ and (b) shows the ratio of the cross section and several predictions to the approximate NNLO [21]. The prediction by ALPGEN is shown as red dashed line, the one from MC@NLO is shown as blue solid line and the prediction at approximate NNLO [21] as green histogram. Within the systematic uncertainties, Fig. 7(b) shows reasonable agreement of the data with the models, while ALPGEN is clearly low in absolute normalization. The distribution for $|y^{\text{top}}|$ is shown in Fig. 8. The ratio in Fig. 8(b) indicates that the distribution is reasonably accommodated by MC@NLO, except at $|y^{\text{top}}|$ of $\approx 0.4 - 1$. The distribution of the data is in marginal agreement with the approximate NNLO prediction (yellow line), but, given the uncertainties it is adequate. Figure 9 (a) shows the unfolded data (black circular markers) as a function of p_T^{top}, compared to the same predictions as discussed in the context of Fig. 7 and Fig. 8. The differential cross section as a function of p_T^{top} is described by MC@NLO and the approximate NNLO QCD prediction. MC@NLO
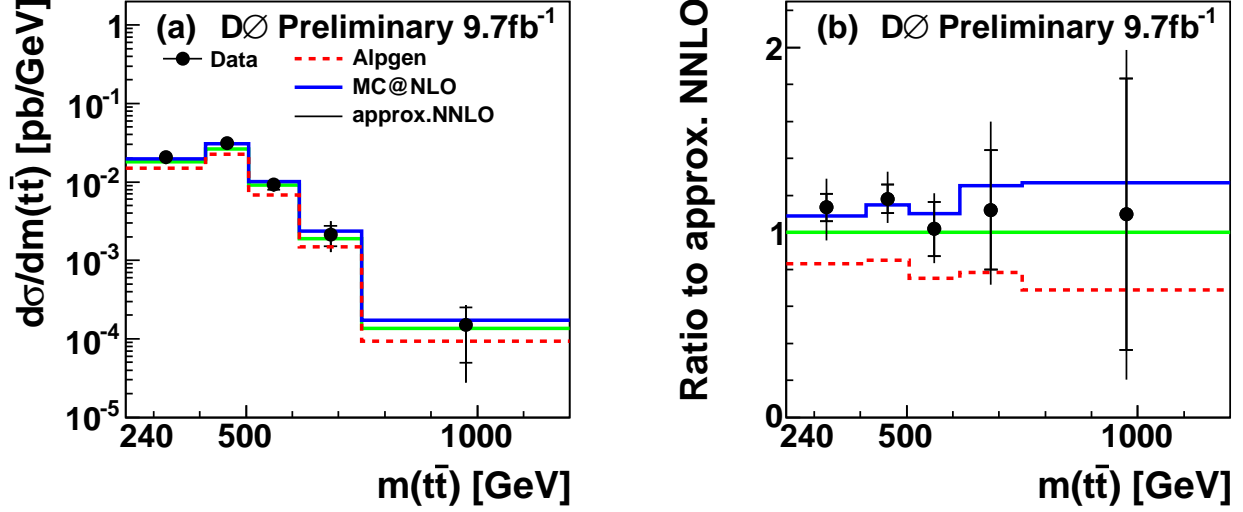
FIG. 7: (a) The differential cross section as a function of $m(t\bar{t})$ for data (black circular markers) compared to several QCD predictions. The inner error bars correspond to the statistical uncertainties and the outer error bars to the systematic uncertainties. (b) The ratio of cross sections to the QCD prediction at approximate NNLO [21]. MC and pQCD predictions use 172.5 GeV unless indicated to the contrary.
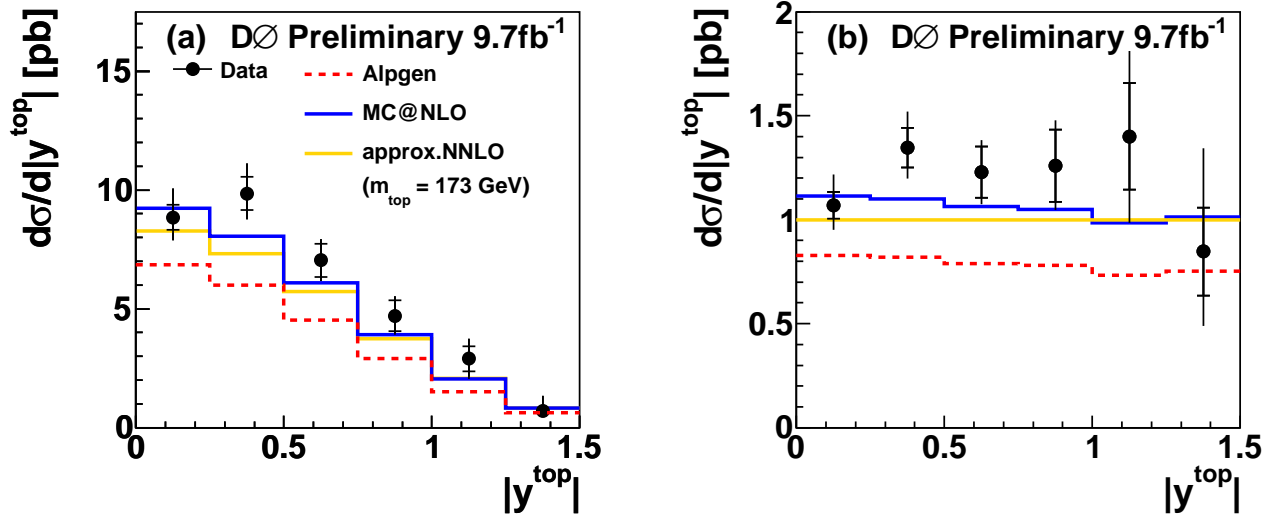

FIG. 8: Differential cross section as a function of $|y^{\text{top}}|$ for data (black circular markers) compared to several QCD predictions. In addition, the approximate NNLO QCD prediction [20] (yellow histogram) is shown for comparison. More details can be found in the caption of Fig. 7.

describes the shape of the p_T^{top} distribution well.

In addition, an earlier measurement by D0 using 1.0 fb^{-1} of data (open squares) is also shown [8]. Statistical uncertainties are defined differently in Ref. [8], and follow Ref. [45], and are not directly comparable with the current uncertainties. The statistical uncertainty of the new D0 result takes into account the effect of bin migrations. The new D0 result shows good agreement with the previous measurement.
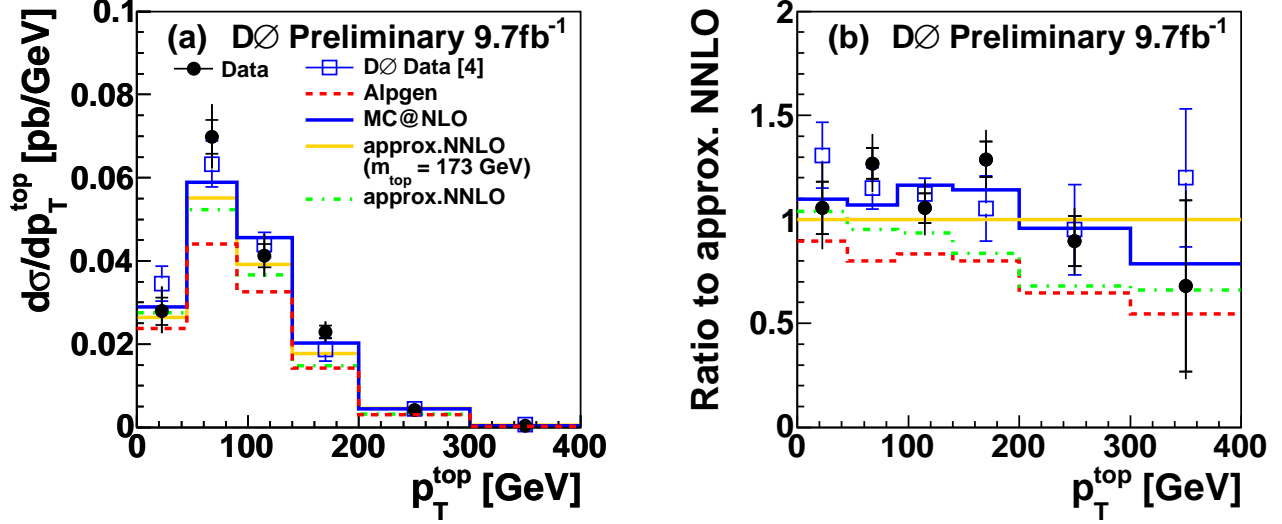
FIG. 9: Differential cross section as a function of p_T^{top} for data (black circular markers). The open squares show the previous D0 measurement [8]. For other details, see captions of Fig. 7 and Fig. 8.

X.   CONCLUSIONS

Differential cross sections for $t\bar{t}$ production are measured in the ℓ+jets decay channels using the full Tevatron Run II data set. The data are corrected for detector efficiency, acceptance and bin migration by means of a regularized unfolding procedure. The differential cross section is measured as a function of the invariant mass of the $t\bar{t}$ system $m(t\bar{t})$, the absolute rapidity of the t and $\bar{t}$ quarks $|y^{\text{top}}|$, and the transverse momenta p_T^{top}. The total inclusive $t\bar{t}$ production cross section extracted from the ℓ+jets decay channel is $\sigma_{\text{tot}}(p\bar{p} \rightarrow t\bar{t}) = 8.27 \pm 0.48(\text{stat.}) \pm_{0.77}^{0.79}$ (syst.) pb. The cross section as a function of p_T^{top} is in good agreement with the previous D0 measurement using 1 fb^{-1}. The differential cross sections are described adequately well by QCD MC generators and predictions at approximate NNLO.

XI.   ACKNOWLEDGEMENTS

[1] CDF Collaboration, F. Abe *et al.*, Phys. Rev. Lett. **74**, 2626 (1995).
[2] D0 Collaboration, S. Abachi *et al.*, Phys. Rev. Lett. **74**, 2632 (1995).
[3] CDF & D0 Collaboration, V. M. Abazov *et al.*, Phys. Rev. D **86**, 092003 (2012).
[4] D0 Collaboration, V. M. Abazov *et al.*, Phys. Rev. D **84**, 112005 (2011).
[5] L. J. Hall and A. E. Nelson, Phys. Lett. B **153**, 430 (1985).
[6] P. H. Frampton and S. L. Glashow, Phys. Lett. B **190**, 157 (1987).
[7] CDF Collaboration, T. Aaltonen *et al.*, Phys. Rev. Lett. **102**, 222003 (2009).
[8] D0 Collaboration, V. M. Abazov *et al.*, Phys. Lett. B **693**, 515 (2010).
[9] N. Kidonakis, Phys. Rev. D **82**, 114030 (2010).
[10] R. Brun and F. Carminati, CERN Program Library Long Writeup W5013 (1993) (unpublished).
[11] S. Frixione and B. R. Webber, J. High Energy Phys. **06**, 029 (2002); S. Frixione *et al.*, J. High Energy Phys. 08, 007 (2003).
[12] G. Corcella *et al.*, J. High Energy Phys. **01**, 010 (2001).
[13] M. L. Mangano *et al.*, J. High Energy Phys. Vol. 2003, No. **07**, pp. 001 (2003).
[14] T. Sjøstrand, S. Mrenna, and P. Skands, J. High Energy Phys. Vol. 2006, No. **05**, pp. 026 (2006).
[15] J. Pumplin *et al.*, J. High Energy Phys. **0310**, 46 (2003).
[16] J. Pumplin *et al.*, J. High Energy Phys. **07**, 12 (2002).
[17] J. Campell, R. K. Ellis, Nucl. Phys. Proc. Suppl. **10** 205 (2010).
[18] F. Deliot, Proc. Top2012, IOP Conference Series (2012).
[19] E. E. Boos, V. E. Bunichev *et al.*, Physics of Atomic Nuclei, 780 (2006).
[20] N. Kidonakis, Phys. Rev. D **84**, 011504(R) (2011).
[21] V. Ahrens *et al.*, J. High Energy Phys. **1009**, 097 (2010).
[22] A. D. Martin, W. J. Stirling, R. S. Thorne, and G. Watt, Eur. Phys. J. C **63**, 189 (2009).
[23] D0 Collaboration, V. M. Abazov *et al.*, Nucl. Instrum. Meth. A **565**, 463 (2006).
[24] S. N. Ahmed *et al*, Nucl. Instrum. Meth. A **634** 8 (2011).
[25] R. Angstadt *et al*, Nucl. Instrum. Meth. A, **622**, 298 (2010).
[26] D0 Collaboration, V. M. Abazov *et al.*, Nucl. Instrum. Meth. A **620**, 490 (2010).
[27] D0 Collaboration, V. M. Abazov *et al.*, Physics Letters **B** 718, pp. 1314-1320 (2013).
[28] D0 Collaboration, V. M. Abazov *et al.*, Phys. Rev. D **74**, 112004 (2006).
[29] D0 Collaboration, V. M. Abazov *et al.*, Phys. Rev. D **84**, 012008 (2011).
[30] D. L. Phillips, J. Assoc. Comp. Mach. 9 **84**, (1962).
[31] A. N. Tikhonov, Soviet Math. Dokl. **4**, 1035 (1963).
[32] V. Blobel, Proc. Advanced Statistical Techniques in Particle Physics, Durham (2002).
[33] E. H. Moore, Bulletin of the American Mathematical Society 26 (9) 394395 (1920).
[34] R. Brun and F. Rademakers, Nucl. Instrum. Meth. A **389**, 81 (1997); S. Schmitt, JINST 7 (2012) T10003 [`arXiv:hep-ph/1205.6201`].
[35] S. Snyder, Doctoral Thesis, State University of New York at Stony Brook (1995).
[36] J. Beringer *et al.* (Particle Data Group), Phys. Rev. D **86**, 010001 (2012).
[37] CDF Collaboration, T. Aaltonen *et al.*, Submitted [`arXiv:hep-ph/1211.1003`].
[38] ATLAS Collaboration, G. Aad *et al.*, Eur. Phys. J. C **73**, 2261 (2013).
[39] CMS Collaboration, S. K. Chatrchyan *et al.*, Submitted [`arXiv:hep-ph/1211.2220`]
[40] D0 Collaboration, V. M. Abazov *et al.*, Phys. Rev. Lett. **101**, 062001 (2008).
[41] D. Meister, Master thesis, University of Illinois Chicago (visitor from ETH-Zürich), [http://e-collection.library.ethz.ch/view/eth:6999] (2012).
[42] T. Andeen *et al.*, FERMILAB-TM-2365 (2007).
[43] P. Baernreuther, M. Czakon and A. Mitov, Phys. Rev. Lett. **109**, 132001 (2012).
[44] M. Guzzi *et al.*, Phys. Rev. D **82**, 074024 (2010).
[45] A. Hoecker and V. Kartvelishvili, Nucl. Instrum. Meth. in Phys. Res. A **372**, 469 (1996).
[46] The letter E is used to signify that the measurement of this observable is based on the calorimetry.

APPENDIX A: CROSS SECTION TABLE

The numerical values of the cross sections are given as a function of $m(t\bar{t})$, $|y^{\mathrm{top}}|$, and p_T^{top} in Tables III, IV, and V, respectively. Contributions beyond the highest bin boundary are included in the last bin of the $m(t\bar{t})$, $|y^{\mathrm{top}}|$ and p_T^{top} distribution.

$m(t\bar{t})$ [TeV/c]	$d\sigma/dM(t\bar{t})$[pb/TeV]	$\delta^{\mathrm{stat.}}$[pb/TeV]	$\delta^{\mathrm{sys.}}$[pb/TeV]
$0.2400 - 0.4125$	20.599	± 1.523	$+3.856$ -3.763
$0.4125 - 0.5050$	31.255	± 2.030	$+0.841$ -2.202
$0.5050 - 0.6150$	9.375	± 1.336	$+0.776$ -0.996
$0.6150 - 0.7500$	2.129	± 0.594	$+0.428$ -0.630
$0.7500 - 1.200$	0.149	± 0.100	$+0.058$ -0.049

TABLE III: Differential cross section as a function of $m(t\bar{t})$. Contributions beyond the highest bin boundary are included in the last bin.

$|y^{\mathrm{top}}|$	$d\sigma/d|y|(t/\bar{t})$[pb]	$\delta^{\mathrm{stat.}}$[pb]	$\delta^{\mathrm{sys.}}$[pb]
$0.00 - 0.25$	8.843	± 0.534	$+0.541$ -0.992
$0.25 - 0.50$	9.837	± 0.700	$+0.515$ -0.870
$0.50 - 0.75$	7.029	± 0.701	$+0.242$ -0.248
$0.75 - 1.00$	4.695	± 0.645	$+0.345$ -0.407
$1.00 - 1.25$	2.959	± 0.532	$+0.561$ -0.581
$1.25 - 1.50$	0.694	± 0.172	$+0.269$ -0.277

TABLE IV: Differential cross section as a function of $|y^{\mathrm{top}}|$. Contributions beyond the highest bin boundary are included in the last bin.

p_T^{top} [TeV/c]	$d\sigma/dp_T(t/\bar{t})$[pb/TeV]	$\delta^{\mathrm{stat.}}$[pb/TeV]	$\delta^{\mathrm{sys.}}$[pb/TeV]
$0.000 - 0.045$	27.764	± 3.311	$+3.207$ -4.291
$0.045 - 0.090$	69.698	± 4.069	$+1.794$ -2.884
$0.090 - 0.140$	41.466	± 2.784	$+3.340$ -3.450
$0.140 - 0.200$	22.835	± 1.507	$+1.250$ -1.335
$0.200 - 0.300$	4.181	± 0.0557	$+0.0405$ -0.0391
$0.300 - 0.400$	0.320	± 0.0197	$+0.0074$ -0.0093

TABLE V: Differential cross section as a function of p_T^{top}. Contributions beyond the highest bin boundary are included in the last bin.